Available online at www.sciencedirect.com
ScienceDirect
Aerosol Science 38 (2007) 823–842
Journal of Aerosol Science
www.elsevier.com/locate/jaerosci

Understanding ion-mobility and transport properties of aerosol nanowires

S.H. Kim[a, b, 1], G.W. Mulholland[a, b], M.R. Zachariah[a, b, *]

[a] *Departments of Mechanical Engineering and Chemistry and Biochemistry University of Maryland, College Park, MD 20742, USA*
[b] *National Institute of Standards and Technology, Gaithersburg, MD 20899, USA*

Received 17 April 2006; received in revised form 5 June 2007; accepted 5 June 2007

Abstract

In a previous experimental study, we demonstrated that gas phase electrophoretic mobility separation enables one to classify diameter-selected carbon nanotubes (CNTs) by length [Kim, S. H. & Zachariah, M. R. (2005). In-flight size classification of carbon nanotubes by gas phase electrophoresis. *Nanotechnology*, *16*, 2149–2152] and have subsequently used this capability to track the growth rate of CNTs in free-flight [Kim, S. H. & Zachariah, M. R. (2006). In-flight kinetic measurements of the aerosol growth of carbon nanotubes by electrical mobility classification. *Journal of Physical Chemistry B*, *110*, 4555–4562]. In this paper, we develop a theoretical model to describe the behavior of nanotubes (or nanowires) undergoing Brownian rotation in an electric field, and provide a more rigorous interpretation of the experimental results. The Boltzmann expression for the orientation probability includes both the free charge energy as well as the polarizability energy. In the theoretical model, we computed the orientation-averaged electrical mobility and the precipitating time of a rotating nanowire in DC electric field in the free-molecular limit. This analysis was used to obtain the precipitation time of a nanowire in a differential mobility analyzer (DMA). Based on the theoretical model and its comparison with experimental measurement, we found that: (i) a stronger electric field was required to select longer nanowires for a given diameter and (ii) shorter nanowires with the aspect ratio of $\beta < \sim 30$ ($d_f = 15$ nm) freely rotate for applied electric field up to ~ 1 kV/cm, while longer nanowires ($\beta > \sim 30$) were aligned by the electric field. The experimentally determined nanowire length was in fair agreement with that computed by our theoretical model, in which the effect of the nanowire's alignment on mobility classification in various electric fields was accounted for. The over prediction of the model for longer nanowires is shown to result from the bent structure of the longer nanowires. The methodology should be generic to other nanostructures with high aspect ratio. Published by Elsevier Ltd.

Keywords: Mobility; Nanowires; Nanotubes; DMA; Modeling

1. Introduction

Size classification of fibrous aerosol particles has been attempted by numerous researchers for realizing either: (i) a preparatory method of fibrous particles with well-defined diameter and length or (ii) a real-time measurement technique of size and length distribution of fibrous aerosol particles (Baron, Deye, & Fernback, 1994; Deye, Gao,

* Corresponding author. Departments of Mechanical Engineering and Chemistry and Biochemistry University of Maryland, College Park, MD 20742, USA. Tel.: +1 301 405 4311; fax: +1 301 314 9477.
E-mail address: mrz@umd.edu (M.R. Zachariah).
[1] Present address: Department of Nanosystem Engineering, Pusan National University, Geumjeong-Gu, Pusan 609-735, South Korea.

0021-8502/$ - see front matter Published by Elsevier Ltd.
doi:10.1016/j.jaerosci.2007.06.003

Baron, & Fernback, 1999; Griffiths, 1988; Lipowicz & Yeh, 1989). Spherical or spherical-like particles may have only one characteristic dimension (e.g. diameter or radius of gyration). The difficulty in characterizing fibers, which by definition have a high aspect ratio, is that both the diameter and length must be determined. If the basis of separation is electrostatics then one has two options. If the object is charged, the electrophoretic motion depends on number of charges on the object, the charge location, and shape. If the object is uncharged, the presence of a strong DC electric field may induce a dipole and result in migration, also known as dielectrophoresis. A number of studies have reported separation of fibrous particles based on length via gas-phase dielectrophoresis (Baron et al., 1994; Deye et al., 1999; Griffiths, 1988; Lipowicz & Yeh, 1989). To achieve dielectrophoretic separation, a strong electric field gradient is required to induce a dipole on micrometer-sized cylindrical-shaped aerosol particles so that they can rapidly align, and migrate in the electric field. Lipowicz and Yeh (1989) found the dielectrophoretic velocity of fibrous particles with diameters in the range of 1–75 μm is proportional to the square of fiber length, and is very weak function of fiber diameter. They therefore concluded that gas-phase dielectrophoresis can separate polydisperse fibers based on length.

In our recent experimental studies (Kim & Zachariah, 2005, 2006) where we employed a differential mobility analyzer (DMA) to measure the mobility size distribution of carbon nanotube (CNT)-laden flows, we found that the role of dielectric separation of gas-phase grown CNTs was negligible, while electrophoretic separation was found to play a key role in mobility size classification of CNTs. These studies showed that singly charged CNTs could be efficiently classified based on length using a DMA (Kim & Zachariah, 2005, 2006).

Several previous studies have used electrophoresis to size classify fibrous aerosols. Zebel, Hochrainer, and Boose (1977) employed an electric mobility spectrometer to separate airborne fibers from spherical-shaped particles. They found that fibrous particles in an electric field deposit on the electrode faster than spherical particles with the same aerodynamic diameter because of higher charge density of fibrous particles. In another work, Chen, Yeh, and Hobbs (1993) employed two steps: (i) classification of fiber diameter using a virtual impactor (aerodynamic diameter of fibers is strongly dependent on fiber diameter), (Stöber, 1972; Timbrell, 1972) and then (ii) classification of fiber length using an electrical aerosol size analyzer (EAA). However, these approaches did not make real-time measurements of fibrous aerosol particles, and they were limited to the electrophoretic separation of fibrous particles in the continuum regime, where the diameter of fibers were larger than ∼3 μm. The definition of continuum size regime for fibrous particles, $Kn = 2\lambda/d_f$ (where λ is the mean free path of the gas, and d_f is the diameter of fiber), follows that suggested by Dahneke (1973), as will be discussed in detail Section 3.

Recently, Moisala, Nasibulin, Shandakov, Jiang, and Kauppinen (2005) in a manner similar to our approach (Kim & Zachariah, 2005, 2006) made an electrophoretic separation for single-walled CNTs (SWCNTs) with ∼6.5 nm in diameter. They state that SWCNTs are preferentially aligned perpendicular to the direction of the electric field. This assertion was based on finding a better agreement between the SWCNTs length measured by TEM and a drag calculation for a perpendicular orientation than for the parallel orientation. Song, Lenggoro, Hayashi, Okuyama, and Kim (2005) also made an electrophoretic separation for electrospray-generated gold nanorod particles with a diameter of ∼13 nm. In their theoretical model, they also considered the behavior of rod-like particles for both perpendicular and random orientation cases in DC electric fields, and then observed significant deviation between experimentally and theoretically determined mobility size of gold nanorod particles due to the presence of a surfactant shell on the each nanorod particle. By including the thickness of surfactant film on the gold nanorod particles (e.g. shell thickness ∼8 nm) in their model, a theoretically determined mobility size of gold nanorod particles was found to agree with the experimentally determined mobility size. They also observed that the initial differences in mobility size estimated by both perpendicular and random orientation cases were significantly decreased with an increasing shell thickness due to the reduction of the aspect ratio.

Our approach to understand the orientation effects on mobility and drag in the DMA comes from a recognition that the orientation of singly charged nanowires in an electric field is strongly affected by electric field, which tries to align the nanowire, and the Brownian motion which tend to randomize the orientation of the nanowire. These two competing effects are a nonlinear function of nanowire length. In the works of both Moisala et al. (2005) and Song et al. (2005), the data were limited to mobility-classified nanorods (or nanotubes) of length less than ∼70 nm (i.e. low aspect ratios less than ∼10) where alignment effects are expected to be minimal.

In this paper, we develop a theoretical model to describe the behavior of nanowires undergoing Brownian rotation in a DC electric field, in order to predict and explain the behavior of nanowires traveling through a DMA. The orientation-averaged mobility of nanowires with various aspect ratio of (up to $\beta = \sim 150$), in various electric fields ($< \sim 5$ kV/cm) is

predicted by the theoretical model developed, and compared with our previously measured results (Kim & Zachariah, 2005).

2. Experimental

Mobility classification of CNTs all with the same diameter was performed in our previous experimental study (Kim & Zachariah, 2005, 2006). Briefly, monodisperse nickel catalyst aerosol nanoparticles were generated by pulsed laser ablation (PLA), followed by size selection with a nano-DMA (Model 3085, TSI, Inc.). The PLA employed a 1064 nm Q-switched Nd:YAG laser, with a pulse width of 4 ns at 10 Hz to ablate a rotating nickel target. A cross-flow of nitrogen, served to carry away the nickel vapor formed in the laser induced plasma as well as to quench the plasma and induce nucleation. These polydisperse nickel aerosol nanoparticles were then introduced into the nano-DMA, whose inlet was modified so as to reside within the ablation chamber as seen in Fig. 1. Since a reasonably high fraction of PLA-generated nickel particles were found to be singly charged no auxiliary charger was necessary. The DMA was operated at ∼1.5 kV, to select mono-area nickel nanoparticle aggregates with a 30 nm mobility size.

These nickel aggregates were then passed thorough a heated flow tube at ∼1200 °C to create fully sintered, isolated single primary particles of ∼15 nm diameter. The sintering kinetics of the size-dependent nickel particles was studied by the use of a tandem DMA, and described in detail elsewhere (Kim & Zachariah, 2007). These sintered nickel aerosol particles, were used as the catalysts for CNT growth, upon addition of acetylene (∼5 sccm) and hydrogen (∼100 sccm) at 750 °C, in a second flow reactor with a nominal growth time of ∼5 s. TEM analysis resulted in a mean and standard deviation for the diameter of ∼14 ± 2 nm, which is close to the DMA-selected particle size of 15 nm. The standard deviation of the diameter measured at several locations within a single CNT was about ±1 nm. The diameter-controlled CNTs flowed through a bipolar charger, based on α particles emitted by Po-210, resulting in an equilibrium charge distribution. The mobility size distribution of the CNTs was measured by the combination of a second DMA and a condensation nucleus counter (CNC).

To interpret the mobility size distribution curve measured by the second DMA, we began with the previously verified assumption that for a freely tumbling object of low fractal dimension, the projected area diameter is equivalent to the

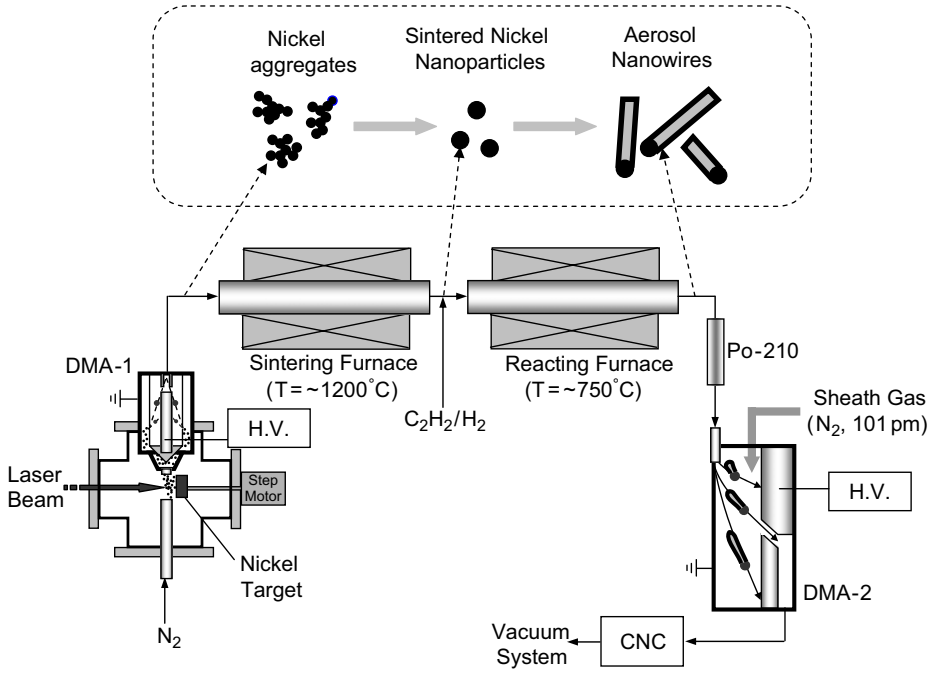

Fig. 1. Schematic of experimental system used for both growth and characterization of aerosol carbon nanotubes (DMA: differential mobility analyzer, CNC: condensation nucleus counter, H.V.: high voltage power supply).

Table 1
Summary of mobility diameter and projected area diameter

t_F (s)	V_e (V)	D_m (nm)	D_A (nm)	β	CNTs length determined by TEM (nm)	t_p (s)	Outermost trajectory ($r_{out} \rightarrow r_b$)		Innermost trajectory ($r_a \rightarrow r_{in}$)	
							β	CNTs length predicted (nm)	β	CNTs length predicted (nm)
2.26	465	50	48 ± 2	8 ± 0.7	121 ± 10	2.26	9	135	9	135
2.26	1093	80	85 ± 4	25 ± 3	378 ± 40	2.26	27	405	27	405
2.26	1614	100	109 ± 5	42 ± 4	622 ± 60	2.26	61	915	61	915
2.26	2199	120	133 ± 6	62 ± 6	926 ± 90	2.26	88	1320	88	1320
2.26	3169	150	167 ± 8	97 ± 10	1460 ± 150	2.26	129	1935	129	1935
2.26	4962	200	226 ± 11	178 ± 17	2674 ± 250	2.26	204	3060	204	3060

Also a comparison between experimentally and theoretically determined CNT length with $d_f = 15$ nm.

mobility diameter (Rogak, Flagan, & Nguyen, 1993; Jung, Kittelson, & Zachariah, 2004). If indeed this were the case for CNTs then the interpretation would be straightforward. To assess the validity of this assumption, we need to know how a cylindrical object moves and rotates in the DMA. Conceptually, in the absence of, or at least at low, electric fields, the random Brownian motion of carrier gas will result in a random orientation of the nanotubes. Such a freely tumbling nanotube will present a drag force proportional to its projected surface area. If so, then mobility classification of diameter-selected CNTs in our experimental approach should be directly proportional to nanotube length. Table 1 presents a summary of our experimental results for the mobility size (D_m) measured by the second DMA, and the projected area diameter (D_A) of CNTs, measured by TEM analysis of the CNTs electrostatically deposited after the second DMA. The experimentally determined nanotube lengths based upon uniform diameter of 15 nm and the DMA mobility measurements are also given in Table 1.

From the measured data presented in the Table 1, it is clear that at low voltages the comparison between the projected area diameter, D_A and the mobility diameter, D_m is excellent. However, as the voltage is increased, essentially selecting longer CNTs, the projected area diameter as determined by TEM is consistently larger than the mobility selected diameter. This effect can be expressed as an increase in the slope for the relationship between D_m and D_A. The best fit linear relationship between D_m and D_A is as follows: $D_A = C_1 D_m + C_2$ where $C_1 = 1.1621$ and $C_2 = -8.9131$. Knowing the value of D_A, one can obtain the nanotube length from the following expression: $L_f = 0.25\pi D_A^2/d_f$. The nanotube length distributions (Table 1) for all six sizes were found to have a standard deviation of about 10% of the mean, which corresponds to a geometric standard deviation of about 1.1. The tightness of the distribution and the quadratic dependence of L_f on the mobility diameter indicate the potential utility of mobility classification of CNTs.

One issue in the TEM analysis is that the projected area of CNTs is changed by a projected angle view by representing a 3d object on a 2d plane. To minimize this error, we have excluded those images in our data analysis CNTs showing significant morphological change when the TEM grid was tilted (up to 45°). This resulted in discarding approximately 10% of the images, which were tubes that were either sitting off the surface at an angle or were significantly bent. In this approach we could view essentially from the side to see in fact if the tube was standing off the substrate.

3. Theoretical model

3.1. Orientation of nanowires undergoing Brownian rotation in an electric field

Fig. 2 illustrates the forces on a cylindrical-shaped particle with hemispherical ends in an electric field. In the absence of turbulence and shear forces, the alignment of singly charged cylindrical particles (e.g. nanotubes or nanowires) depends on the alignment energy from the electric field and thermal energy associated with the Brownian motion. The former will cause the fiber to align in the field while the latter will induce a random orientation. Fig. 2 also defines the geometric specifications of the DMA. We have employed a simplified plug flow DMA model with virtual inlet and outlet slits, which have no effect on the flow. A certain fraction of aerosol flow goes through inlet slit located in r_a, and then the equal fraction of aerosol flow goes through the outlet slit located in r_b (Hagwood, Sivathanu, & Mulholland,

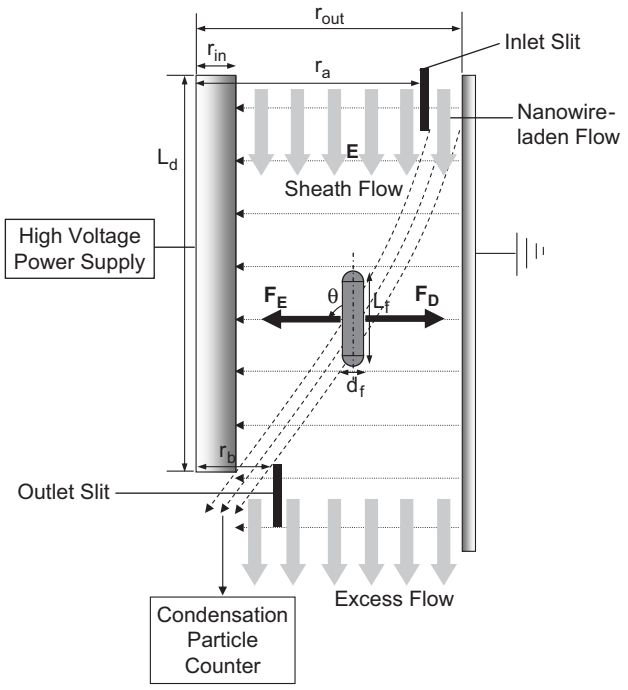

Fig. 2. Schematic of the behavior of cylindrical-shaped particle in an electric field, and notations used in the models.

1999). The transfer function obtained using our model is identical with that obtained by Hagwood et al. (1999) and Knutson & Whitby (1975) for any laminar flow.

The orientation energy arises from two field dependent effects: one from the charged nanowire and the second from the polarizability of the nanowire.

3.1.1. Electrophoretic effect

The electrical energy for the first effect is computed assuming that the positive charge is located at the end of the nanowire closest to the lowest voltage electrode. The force acting on the nanowire is the product of the electric field and the charge. The magnitude of the resulting torque τ is given by

$$\tau = \tfrac{1}{2}\, L_{\mathrm{f}} neE \sin\theta, \tag{1}$$

where n is the number of elementary units of charge, e is the elementary electrical charge, E is the electric field intensity, and θ is the angle between the direction of the electric field and the axis of the nanowire. The change in the electrical energy Φ_q resulting from the rotation of a charged nanowire by an angle θ is given by

$$\Phi_q = \int_0^{\theta} \tau \,\mathrm{d}\theta = \frac{L_{\mathrm{f}}}{2}\, qE(1-\cos\theta). \tag{2}$$

3.1.2. Dielectrophoretic effect

The second term arises from the polarizability of the nanowire. We approximate the electrical energy of a polarizable cylinder Φ_{p} with that of a polarizable prolate spheroid with the same volume as the cylinder and with the same aspect ratio. The aspect ratio for the cylinder β is the ratio of the cylinder length to the cylinder diameter and for the ellipsoid it is the ratio of the major and minor semi-axes, a/b. For these constraints, the relationship between the minor semi-axis b and the diameter d_{f} of the cylinder is given by

$$b = (\tfrac{3}{16})^{1/3} d_{\mathrm{f}}. \tag{3}$$

The following expression is given by Fuchs (1964) for the energy of a polarizable, prolate ellipsoid in an electric field

$$\Phi_{\mathrm{p}} = -\frac{1}{2}(2\pi\varepsilon_0)\Sigma E^2\left[\frac{\cos^2\theta}{(1/(\varepsilon_k-1))+\kappa_1}+\frac{\sin^2\theta}{(1/(\varepsilon_k-1))+\kappa_2}\right], \tag{4}$$

where ε_0 equals the permittivity in free space, ε_k is the dielectric constant of the particle, Σ is the volume of the prolate ellipsoid with a major semi-axis a and minor semi-axis b, and κ_1 and κ_2 are the shape factors. The expressions for the shape factors are given by

$$\kappa_1 = \frac{1}{\beta^2-1}\left[\frac{\beta}{\sqrt{\beta^2-1}}\ln\left(\beta+\sqrt{\beta^2-1}\right)-1\right], \tag{5}$$

$$\kappa_2 = \frac{\beta}{2(\beta^2-1)}\left[\beta-\frac{1}{\sqrt{\beta^2-1}}\ln\left(\beta+\sqrt{\beta^2-1}\right)\right]. \tag{6}$$

In the case of conducting particles, such as those considered here, the large value of the dielectric constant when used in Eq. (4) ($\varepsilon_k \gg 1$) makes the electrical energy due to polarization, essentially independent of material with the term $1/(\varepsilon_k - 1)$ set equal to 0.

The total orientation electrical energy Φ_{t} is obtained from Eqs. (2) and (4) as follows:

$$\Phi_{\mathrm{t}} = \frac{L}{2}qE(1-\cos\theta)-\frac{1}{2}(2\pi\varepsilon_0)\Sigma E^2\left[\frac{\cos^2\theta}{\kappa_1}+\frac{\sin^2\theta}{\kappa_2}\right]. \tag{7}$$

It is convenient to define a reduced energy as the energy divided by the Brownian rotation energy kT. For $\beta \gg 1$, the first term in Eq. (7) is proportional to β while the second term is proportional to $\beta^3/\ln\beta$. For smaller β and E, the first term dominates the total electrical energy, while for large β and E, the second term dominates. This effect is illustrated in Fig. 3 for $\beta = 8$ and 42 for $d_{\mathrm{f}} = 15$ nm. The fields correspond to the peak number, for the nanowires passing through the DMA.

This energy ratio is a convenient measure of the tendency of the nanowire to align in the electric field. If the Brownian rotation energy kT is greater than the electrical energy, then the orientation of the nanowire will be random. We use the following energy difference in computing the energy ratio $E_{\mathrm{e}}/E_{\mathrm{B}}$:

$$\frac{E_{\mathrm{e}}}{E_{\mathrm{B}}} = (\Phi_{\mathrm{t}}(\pi/2)-\Phi_{\mathrm{t}}(0))/kT. \tag{8}$$

Fig. 4 presents the relative electrical energy to Brownian rotation energy (Eq. (8)) as a function of applied electric field intensity, and aspect ratio for nanotubes. The critical value of the relative electrical energy to Brownian rotation energy was chosen to be $E_{\mathrm{e}}/E_{\mathrm{B}} = 10$ for determining the wires alignment as suggested by Fuchs (1964). It is seen that for the smallest β taken from Table 1, the orientation is expected to be nearly random, and for the three values of $\beta \geqslant 60$ the orientation is predicted to be nearly aligned. For the intermediate values some measure of the extent or probability of alignment is required.

The probability of alignment at polar angle θ and azimuthal angle ϕ, $\Pi(\theta, \phi)$ is given by Boltzmann's law (Fuchs, 1964).

$$\Pi(\theta,\phi)\,\mathrm{d}\Omega = \Pi(\theta,\phi)\sin\theta\,\mathrm{d}\theta\,\mathrm{d}\phi = c\exp[-\Phi_{\mathrm{t}}/kT]\sin\theta\,\mathrm{d}\theta\,\mathrm{d}\phi, \tag{9}$$

where Ω is the solid angle and a normalization constant c. As seen from Eq. (7), the electrical energy depends on only the angle θ so that the orientation probability $P(\theta)$ can be expressed as

$$P(\theta)\,\mathrm{d}\theta = c\exp(\Phi_{\mathrm{t}}/kT)\sin\theta\,\mathrm{d}\theta, \tag{10}$$

with the normalization condition,

$$\int_0^{\pi/2} P(\theta)\,\mathrm{d}\theta = \int_0^{\pi/2} c\exp(-\Phi_{\mathrm{t}}/kT)\sin\theta\,\mathrm{d}\theta = 1. \tag{11}$$

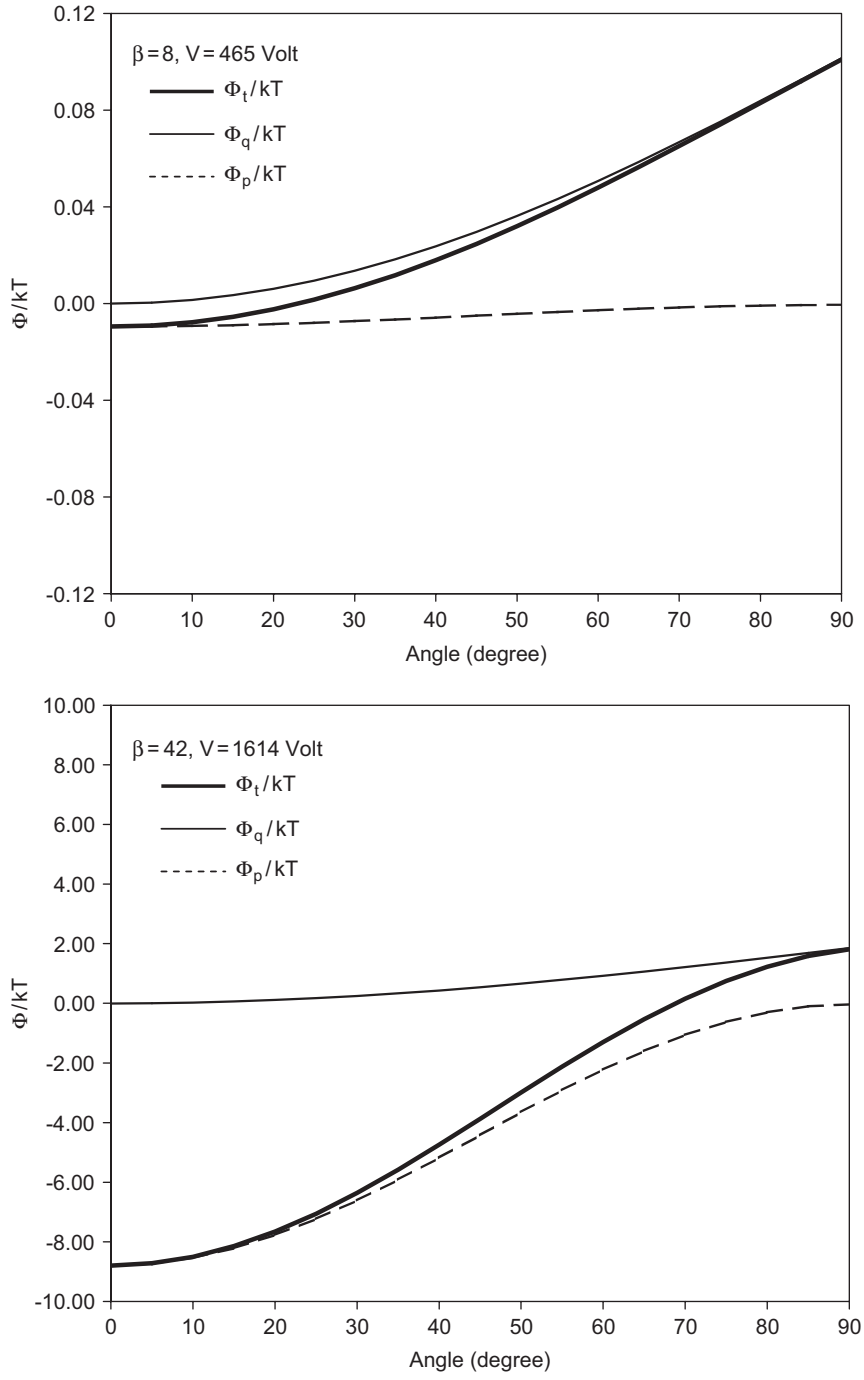

Fig. 3. Relative electrical field energy (q), polarizable energy (p), and total energy (t) to the Brownian motion energy as a function of rotating angle.

The upper limit of the integration is $\pi/2$ because the positive charge on the nanowire always remains at the end of the nanowire closest to the electrode with the lowest voltage.

It is useful to change the independent variable from θ to $x = \cos\theta$ for Eq. (10).

$$P(\theta)\,\mathrm{d}\theta = P(\theta)\frac{\mathrm{d}\theta}{\mathrm{d}x}\,\mathrm{d}x = \frac{cP(\theta)}{-\sin\theta}\,\mathrm{d}x. \tag{12}$$

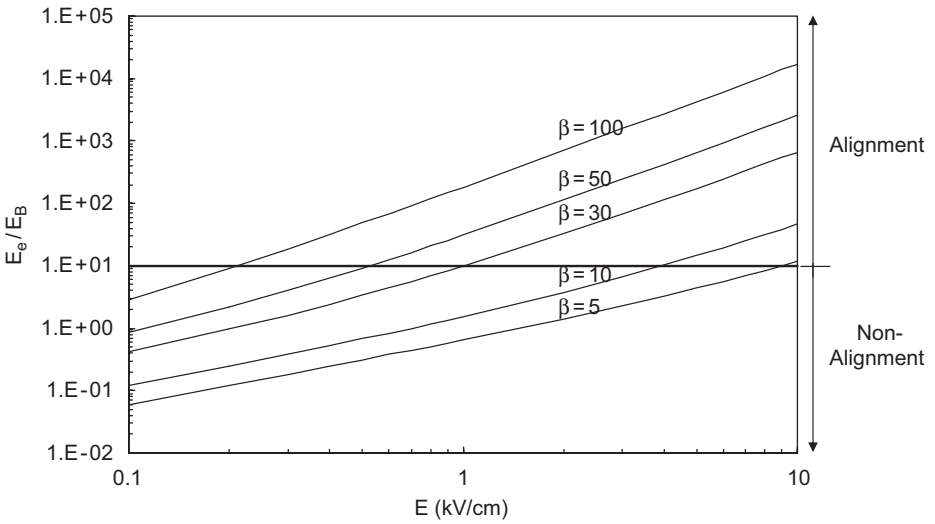

Fig. 4. Relative electrical energy to Brownian rotation energy as a function of applied electric field, and aspect ratio for nanowires (nanowire diameter, d_f, was assumed to be 15 nm).

Substituting for $P(\theta)$ from Eq. (10), we obtain

$$P(\theta)\,\mathrm{d}\theta = -c\exp(-\Phi_t/kT)\,\mathrm{d}x = -P_1(x)\,\mathrm{d}x, \tag{13}$$

with the normalization condition

$$\int_0^1 P_1(x)\,\mathrm{d}x = \int_0^1 c\exp(-\Phi_t/kT)\,\mathrm{d}x = 1. \tag{14}$$

Substituting the expression for Φ_t from Eq. (7) into Eq. (13) and using $x = \cos\theta$ as the independent variable we obtain:

$$P_1(x)\,\mathrm{d}x = c\exp\left[-\frac{L}{2}\frac{qE}{kT} + \frac{\pi\varepsilon_0\Sigma E^2}{\kappa_2 kT}\right]\exp\left[\frac{L}{2}\frac{qEx}{kT} + \frac{\pi\varepsilon_0\Sigma E^2x^2}{kT}\left(\frac{1}{\kappa_1}-\frac{1}{\kappa_2}\right)\right]\mathrm{d}x. \tag{15}$$

To make the β dependence explicit in the right-hand side of Eq. (15), we express L and Σ as functions of β and d.

$$L = \beta d_f, \tag{16}$$

$$\Sigma = \beta\frac{\pi}{4}d_f^3. \tag{17}$$

Substituting from Eqs. (16) and (17) into Eq. (15) and introducing simplifying combinations of constants, we obtain:

$$P_1(x)\,\mathrm{d}x = c\exp(-\alpha_1\beta E + \alpha_3\beta E^2)\exp(\alpha_1\beta Ex + \alpha_2\beta E^2x^2)\,\mathrm{d}x, \tag{18}$$

where

$$\alpha_1 = \frac{d_f q}{2kT}, \tag{19}$$

$$\alpha_2 = \frac{\pi\varepsilon_0\pi d_f^3}{4kT}\left(\frac{1}{\kappa_1}-\frac{1}{\kappa_2}\right), \tag{20}$$

$$\alpha_3 = \frac{\pi\varepsilon_0\pi d_f^3}{4kT\kappa_2}. \tag{21}$$

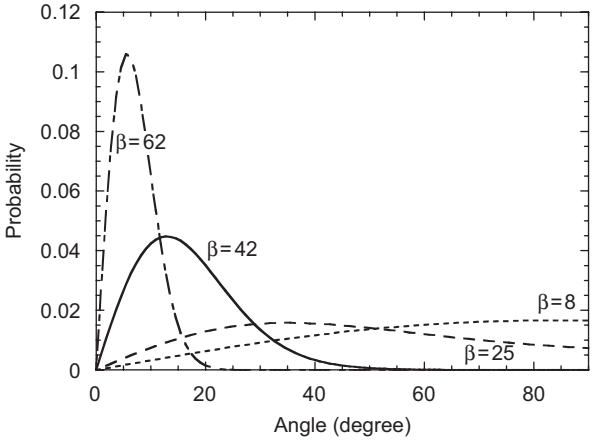

Fig. 5. Effect of aspect ratio on the probability distribution for nanowires with a 15 nm diameter and for electric fields of 0.45 kV/cm ($\beta = 8$), 1.05 kV/cm ($\beta = 25$), 1.55 kV/cm ($\beta = 42$), and 2.11 kV/cm ($\beta = 62$).

The next step is to determine the normalization constant c from Eqs. (14) and (18).

$$\frac{1}{c} = \exp(-\alpha_1 \beta E + \alpha_3 \beta E^2) \int_0^1 \exp(\alpha_1 \beta E x + \alpha_2 \beta E^2 x^2)\, \mathrm{d}x. \tag{22}$$

The integration can be performed by completing the square and expressed in terms of the imaginary error function, *Erf*i.

$$c = \frac{(4E^2\alpha_2\beta/\pi)^{1/2} \exp[(\alpha_1^2\beta/4\alpha_2) + \beta E(\alpha_1 - \alpha_3 E)]}{Erfi[(\alpha_1 + 2\alpha_2 E)\beta^{1/2}/2\alpha_2^{1/2}] - Erfi[\alpha_1\beta^{1/2}/2\alpha_2^{1/2}]}, \tag{23}$$

where

$$Erfi(x) = Erf(\mathrm{i}x) = \frac{2}{\pi} \int_0^{ix} \mathrm{e}^{-t^2}\, \mathrm{d}t.$$

Substituting this expression for c in Eq. (18), the following result for P_1(x) is obtained:

$$P_1(x)\, \mathrm{d}x = \frac{(4E^2\alpha_2\beta/\pi)^{1/2} \exp[\alpha_1^2\beta/4\alpha_2] \exp(\alpha_1\beta E x + \alpha_2\beta E^2 x^2)}{Erfi[(\alpha_1 + 2\alpha_2 E)\beta^{1/2}/2\alpha_2^{1/2}] - Erfi[\alpha_1\beta^{1/2}/2\alpha_2^{1/2}]}\, \mathrm{d}x. \tag{24}$$

In the limit where their is only a charged nanowire, and no polarizability term (α_2 and α_3 both equal 0), the following expression for $P_1(x)$ is obtained:

$$P_1(x) = \frac{\alpha_1\beta E}{(\exp(\alpha_1\beta E) - 1)} \exp(\alpha_1\beta E). \tag{25}$$

For comparing with DMA measurements, the probability functions are computed for values of β corresponding to the values obtained by TEM analysis and for the electric fields corresponding to the average field for the peak concentration for the nanowires exiting the DMA. As β increases the probability function $P(\theta)$ goes from a broad distribution with a peak near 90° ($\beta = 8$) to narrow distribution with a peak around 6° ($\beta = 62$) as shown in Fig. 5. The behavior of the other probability function P_1 $(\cos\theta)$ is also of interest. As seen from Eq. (13), $P_1(\theta)$ is independent of $\cos\theta$ for small β and has a peak near $\cos\theta = 1$ for large β. In the limit of small β, for which the nanowire rotates randomly, the average value of θ is computed from Eq. (10) with the exponential equal 0.

$$\overline{\theta} = \frac{\int_0^{\pi/2} \theta \sin\theta\, \mathrm{d}\theta}{\int_0^{\pi/2} \sin\theta\, \mathrm{d}\theta} = 1 \text{ rad } (57.3°).$$

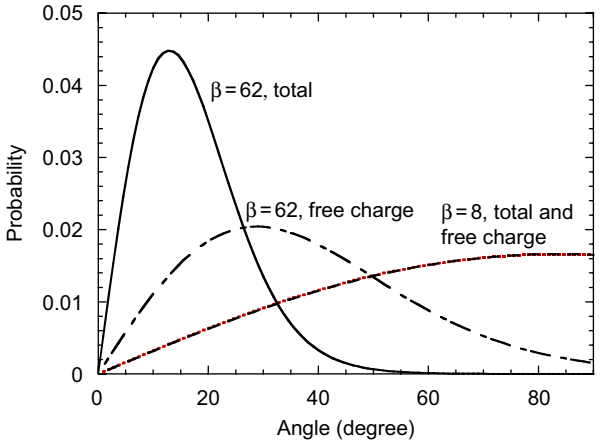

Fig. 6. Comparison of probability for free charge and for combined charge and polarizability for electric fields of 0.45 kV/cm ($\beta = 8$) and 2.11 kV/cm ($\beta = 62$).

The average value of $\cos\theta$, which is randomly distributed over the interval 0–1, is 0.5. In the limit of long wires and high fields, the nanowires become oriented with an average θ approaching 0 and an average $\cos\theta$ approaching 1.

As one can see in Fig. 4 for $d_f = 15$ nm, nanowires with an aspect ratio of $\beta < \sim 30$ should freely rotate regardless of applied electric field up to ~ 0.7 kV/cm. However, nanowires with higher aspect ratio, $\beta > \sim 50$ can be forcedly aligned by even relatively weak electric fields higher than ~ 1 kV/cm. This implies that free-flight nanowires with relatively small aspect ratio ($\beta < \sim 30$) experiences Brownian dynamical forces which result in freely rotating motion of nanowires. A freely rotating nanowire will present a drag force proportional to its projected surface area. Furthermore, since we selected diameter-controlled nanowires in our experimental approach, the second mobility classification of nanowires with uniform diameter would therefore only be a function of length. This conceptual model was verified in our experimental study (Kim & Zachariah, 2005) that in fact nanowires with uniform length were classified at each fixed applied voltage corresponding to an equivalent mobility size. However, as seen in Table 1, the deviation between projected area diameter (D_A) and mobility diameter (D_m) increased with increasing electric field. Since the project area diameter was always larger than the mobility diameter, this implies that at the higher voltages the effective drag on the nanowire was smaller so that a longer nanowire was passed through the DMA. Another way to consider this is that the apparent mobility increases at higher voltages for longer nanowires, and is an indication of alignment effects occurring in the DMA.

The dominance of the charged nanowire energy for small β and small E on the orientation probability and the polarizability energy for large β and large E is illustrated in Fig. 6. These plots are for a fixed nanowire diameter of 15 nm. As the diameter is decreased, the charge energy will dominate since it is proportional to d_f while the polarizability energy is proportional to d_f^3; on the other hand, the polarizability energy will dominate for large E because of the E^2 dependence compared to the linear dependence for the charged nanowire energy.

3.2. Derivation of electrical mobility of rotating nanowires in an electric field

We now turn our attention to developing a theoretical model to describe the motion of nanowires undergoing Brownian rotation in an electric field. When a singly charged nanowire is introduced into a DMA, it is attracted toward the opposite polarity electrode by an electrostatic attraction force (F_E), and simultaneously retarded by the drag force (F_D). The electrostatic attraction force is expressed by

$$F_E = neE, \tag{26}$$

where n is the number of charge on nanowire, and e is the elementary electrical charge. Eq. (26) leads to the electrophoretic velocity, and for the forgoing discussion of the separation of nanowires we ignore dielectrophoretic effects. The justification is based on a lack of any evidence in our experiments that dielectrophoretic plays a role, beyond

alignment effects. In general, the dielectrophoretic velocity is proportional to the gradient in the electric field, which for a DMA is relatively small, except very close to the center electrode. For example for a 20 nm × 10 μm conducting fiber in a 30,000 Vcm field we estimate a dielectrophoretic velocity $\sim 10^{-5}$ cm/s and an electrophoretic velocity ~ 0.1 cm/s. As such one can conclude that while dielectrophoresis may play an important role in alignment of the wire, it is relatively unimportant in the regimes considered in the DMA for actual separation relative to electrophoresis.

For the drag force we use the results developed by Dahneke (1973) for a cylindrical particle with hemispherical ends in free molecular regime as shown below:

$$F_D = \frac{\pi \eta d_f V_r}{Kn}\left[\left(\beta f + \frac{\pi f}{6} + \frac{4}{3}\right) + \beta\left(2 - \frac{6-\pi}{4} f\right)\sin^2\theta\right], \tag{27}$$

where η is the gas viscosity, Kn is the Knudsen number ($=2\lambda/d_f$), λ is the mean free path of gas, d_f is the nanowire diameter, V_r is the particle velocity in radial direction, f is the momentum accommodation coefficient ($=0.9$), T is the absolute temperature, and θ is the angle between the axis of the cylinder and the direction of particle motion (see Fig. 2).

By equating the two forces in Eqs. (26) and (27) and solving for the electrical mobility, Z_p, which is equal to V_r/E, we obtain:

$$Z_p = \frac{ne\,Kn}{\pi\eta d_f[(\beta f + (\pi f/6) + \frac{4}{3}) + \beta(2 - ((6-\pi)/4) f)\sin^2\theta]}. \tag{28}$$

For large β, the mobility increases by about 70% as the nanowire orientation is changed from perpendicular to the field to parallel to the field.

The electrical mobility for these cylindrical particles may also be defined for the particular experimental DMA configuration as a function of DMA geometry, total volumetric gas flow rate, and applied voltage as follows:

$$Z_p = \frac{Q_{sh}\ln(r_{out}/r_{in})}{2\pi V_e L_d}, \tag{29}$$

where Q_{sh} is the sheath flow rate, r_{in}($=0.937$ cm) and r_{out} ($=1.961$ cm) are the inner and outer radii of annular gap space in a DMA, V_e is the applied potential, and L_d is the length of DMA electrode ($=44.369$ cm). The derivation of electrical mobility of a particle (i.e. Eq. (29) based on a simplified DMA configuration (see Fig. 2)) is presented in Appendix A.

By equating Eqs. (28) and (29) we obtain the length of a cylindrical particle, L_f, with diameter, d_f, and fixed orientation θ that would exit the classifier with an applied voltage V_e as shown below:

$$L_f = \frac{(2ne\lambda/\pi\eta d_f^2)(2\pi V_e L_d/Q_{sh}\ln(r_{out}/r_{in})) - ((\pi f/6) + \frac{4}{3})}{1/d_f\left(f + (2 - (((6-\pi) f)/4))\sin^2\theta\right)}. \tag{30}$$

Even though the actual nanowire is rotating, the value of L_f given by Eq. (30) provides a convenient qualitative estimate of the effect of orientation. Fig. 7 presents a mapping of experimentally determined CNTs' length onto theoretically calculated CNTs' length (Eq. (30)) to extract the average extent of CNTs alignment. The solid lines (theoretical model) are each for a fixed applied voltage.

So for any given applied voltage, nanowires aligned perpendicular to the field will have a higher drag, and therefore a smaller nanowire will pass through the DMA. As the alignment angle shallows the effective drag decreases and therefore a longer nanowire will have the same observed mobility. If we now map our experimental observation onto this graph we can obtain an approximate measure of the extent of alignment. The data points represent the TEM measured CNT length at a specific DMA voltage. So for example at 4.96 kV, TEM observation gives a length of 2674 ± 250 nm. If we place that data point on the solid curve, we find this theoretically corresponds to an average angle of the nanowire with respect to the field of $\sim 18 \pm 7°$, and therefore implies a highly aligned nanowire. In contrast, at the lowest voltage of 0.47 kV using the same mapping exercise, we get a value for the nominal angle of $\sim 57°$. At intermediate values of voltages the mapping exercise gives angles that are a monotonic function of applied voltage, and imply that the transition from freely rotating to random configuration is a continuum.

For a freely rotating cylindrical object, the average of $\sin^2\theta$ is given by (Fuchs, 1964)

$$\langle \sin^2\theta \rangle = \tfrac{2}{3}(1 - \exp(-6kT B_\omega t)), \tag{31}$$

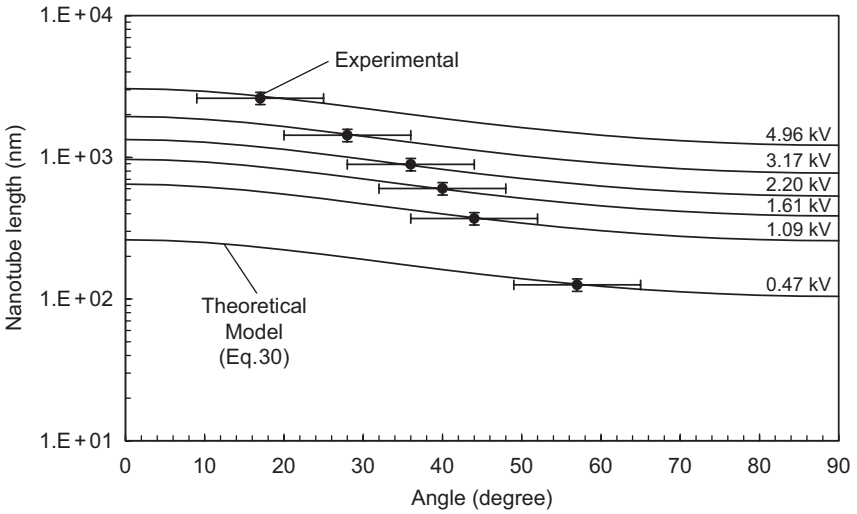

Fig. 7. Comparison of experimentally determined CNTs' length with theoretically calculated CNTs' length (each applied voltages to DMA correspond to mobility size of 50 nm (=0.47 kV), 80 nm (=1.09 kV), 100 nm (=1.61 kV), 120 nm (=2.20 kV), 150 nm (=3.17 kV), and 200 nm (=4.96 kV) where DMA geometry considered was $r_{in} = 0.937$ cm (electrode radius), $r_{out} = 1.961$ cm (radius of housing), $L_d = 44.369$ cm (electrode length), and $Q_{sh} = 10$ lpm (sheath flow rate)). Solid lines are curves of constant mobility.

where t is the CNT flight time in the DMA (~2.3 s). The quantity B_ω is the free molecular rotational mobility, which is a function of the aspect ratio of a cylindrical particle and carrier gas viscosity, and is given by the approximate expression,

$$B_\omega = \frac{48\lambda}{k\pi\eta d_f^4 \beta^3}. \tag{32}$$

The derivation is presented in Appendix B. The term involving B_ω in Eq. (31) is vanishing small after 3 s for aspect ratios of $\beta = 10$–200 (with $d_f = 15$ nm), and the computed average angle is ~55°, which is very close to the angle of $57 \pm 7°$ for 126 ± 10 nm long nanowires classified at 0.47 kV (mobility size of 50 nm). This indirectly indicates that shorter lengths rotate relatively freely regardless of the applied electric field up to ~5 kV/cm, where the relative thermal energy to electric field seems to be sufficient to randomize the nanowire's rotation.

3.3. Mobility classification of in-flight carbon nanowires with uniform diameter

Inspection of Eq. (30) indicates that the classified nanowire length is a function of rotating angle at fixed applied voltage. However, Eq. (30) is not useful to directly predict nanowire length classification by a DMA as long as the rotation angle is undetermined. Furthermore, since in a cylindrical geometry, common to most DMAs, the electric field varies with radial location, the minimum energy orientation of the nanowire will depend on the radial location.

In developing a deterministic theoretical model there are three steps to compute the nanowire length classified by the DMA. The first step is to compute the orientation-averaged mobility as a function of nanowire length and electric field. The second step is to compute the time for a nanowire of specified length to travel from the outer diameter to the inner diameter given a fixed inner electrode voltage. The third step is to adjust the value of the nanowire length, until the precipitating time is equal to the fluid transit time. This nanowire length should correspond to nanowire passing through the DMA for each experimental voltage.

We begin by deriving the orientation-averaged electrical mobility. The orientation-averaged mobility is basically the angle dependent mobility weighted by the probability of a nanowire having a given angle.

$$\overline{Z_p} = \int_0^{\pi/2} Z_p(\theta) P(\theta)\, d\theta = \int_0^1 Z_p(x) P_1(x)\, dx. \tag{33}$$

From Eqs. (24) and (28), we derive the orientation-averaged electrical mobility of a rotating nanowire:

$$\overline{Z_p(E,\beta)} = \int_0^1 \frac{k_1(4E^2\alpha_2\beta/\pi)^{1/2}}{\beta f + k_2 + \beta k_3(1-x^2)} \frac{\exp[\alpha_1^2\beta/4\alpha_2]\exp(\alpha_1\beta E x + \alpha_2\beta E^2 x^2)}{Erfi[(\alpha_1+2\alpha_2 E)\beta^{1/2}/2\alpha_2^{1/2}] - Erfi[\alpha_1\beta^{1/2}/2\alpha_2^{1/2}]}\,dx, \tag{34}$$

where

$$k_1 = \frac{neKn}{\pi\eta d_f}, \quad k_2 = \frac{\pi f}{6} + \frac{4}{3} \quad \text{and} \quad k_3 = \left(2 - \frac{6-\pi}{4} f\right).$$

We note that the orientation averaged mobility is a function of only the electric field and the aspect ratio for a fixed nanowire diameter.

The orientation-averaged mobility is statistically valid if a nanowire rotates by at least 2π, while flowing through the DMA. We calculate the mean square angle of Brownian rotation in a given time, t_r, using the equation for rotational Brownian motion (Fuchs, 1964):

$$\overline{\theta^2} = 2k_B T B_\omega t_r. \tag{35}$$

From the combination of Eqs. (13) and (16), the time required for a nanowire to rotate through an angle of 2π, t_r, is computed as a function of the aspect ratio: ~0.001 ms ($\beta = 5$), 1 s ($\beta = 50$), 10 ms ($\beta = 100$), and 30 ms ($\beta = 150$). Since the rotation time calculated above is much smaller than the precipitation time (~2.3 s) regardless of aspect ratio, Eq. (34) is a valid expression for the orientation-averaged mobility for the conditions in the DMA.

The second step of the analysis is to compute the time (t_p) for the nanowire to travel from the location of inlet slit to the location of outlet slit. As seen in Fig. 2, we choose both outermost and innermost particle trajectories, which have a transfer function of unity for spherical particles (Jung et al., 2004). Here the transfer function is defined as the probability that an aerosol entering from inlet slit will exit through outlet slit. Thus, this precipitation time is equal to the following integrals:

$$t_{p,o} = \int_{r_b}^{r_{out}} \frac{dr}{v_r} \quad \text{(i.e. outermost trajectory)}, \quad t_{p,i} = \int_{r_{in}}^{r_a} \frac{dr}{v_r} \quad \text{(i.e. innermost trajectory)}. \tag{36}$$

The CNT velocity in the radial direction (v_r) is equal to the product of the electric field and the orientation averaged mobility ($= \overline{Z_p(E,\beta)}\cdot E$). Using Eq. (34) for the average mobility and making use of the r dependence of the electric field, $E = V_e/r\ln(r_{out}/r_{in})$, one can express for t_p with E as the integration variable:

$$t_{p,o} = \frac{V_e}{\ln(r_{out}/r_{in})} \int_{E_{out}}^{E_b} \frac{dE}{E^3\overline{Z_p(E,\beta)}}, \quad t_{p,i} = \frac{V_e}{\ln(r_{out}/r_{in})} \int_{E_a}^{E_{in}} \frac{dE}{E^3\overline{Z_p(E,\beta)}}. \tag{37}$$

The third step of the analysis is to determine the value of β for fixed limits of the electric field that will yield a precipitation time t_p computed by Eq. (37) equal to the fluid transit time (t_F) taken for the CNT-laden gas traveling from the top of the DMA to the bottom exit slit. The expression for t_F is as follows:

$$t_F = \frac{\pi(r_{out}^2 - r_{in}^2)L_d}{Q_{total}}, \tag{38}$$

where Q_{total} is the total flow rate (i.e. $Q_{total} = Q_a + Q_{sh}$, where Q_a is the aerosol flow rate). From the DMA geometry and total volumetric gas flow rate, t_F is calculated to be ~2.26 s from Eq. (38) for our experimental conditions.

If the integration in Eq. (37) is carried out for a spherical particle, and if t_F is equal to t_p, one can obtain an expression for the electrical mobility identical to Eq. (29). The derivation of this result is shown in Appendix A. This demonstrates the appropriateness of the integration limits from r_b to r_{out} and r_{in} to r_a.

To evaluate the precipitation time of a nanowire in Eq. (37), one should first calculate the orientation-averaged mobility (i.e. Eq. (34)), which is a function of electric field and aspect ratio. Here we employed the Gaussian quadrature numerical integration method (Hoffman, 2001) to calculate orientation-averaged mobility as a function of electric field with a selected aspect ratio. Second the orientation-averaged mobility is applied in Eq. (37) to evaluate precipitation time of the nanowire for a selected aspect ratio and electric field strength range determined by the DMA geometry and

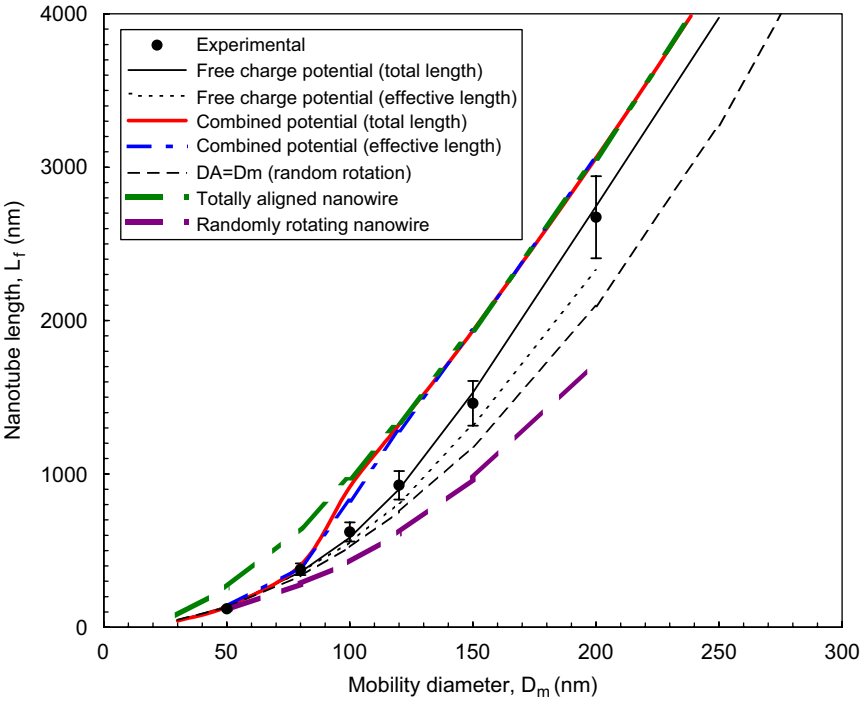

Fig. 8. Comparison of experimentally determined nanowire length with theoretically predicted nanowire based on free charge potential and combined potential (i.e. free charge+polarization) as a function of mobility diameter. The ±1 sigma uncertainty limits for the measurements are shown.

the applied voltage. These numerical calculations for Eqs. (34) and (37) were repeated for a range of aspect ratios at each electric field strength condition until the precipitation time was equal with the fluid transit time.

The predicted results for L_f versus D_m for a 15 nm diameter nanowire are given in Table 1 and Fig. 8. In the limits of either random orientation (small L_f), or full alignment (large L_f) explicit expressions can be derived for the relationships. In the limit of random orientation, $P_1(x) = 1$, and $\overline{Z}_p$ can be expressed as

$$\overline{Z}_p = \int_0^1 Z_p \, dx = \frac{k_1}{\beta(f + k_3) + k_2} \int_0^1 \frac{dx}{(1 - a^2x^2)} = \frac{k_1 \ln[(1 + a)/(1 - a)]}{2a(\beta(f + k_3) + k_2)}, \tag{39}$$

where

$$a = \left(\frac{\beta k_3}{\beta(f + k_3) + k_2} \right). \tag{40}$$

Equating $\overline{Z}_p$ to the mobility of a sphere, which corresponds to the DMA diameter D_m, we find:

$$\frac{D_m}{C(D_m)} = \frac{d_f^2 a(\beta(f + k_3) + k_2)}{3\lambda \ln[(1 + a)/(1 - a)]}, \tag{41}$$

where λ is the mean free path and $C(D_m)$ is the Cunningham slip correction. This provides an implicit relationship between β (or L_f) and D_m. For each of the six values of D_m in Table 1, the value of L is computed and plotted in Fig. 8. In the common case of a long aspect ratio where $\beta(f + k_3) \gg k_2$ so that the k_2 term can be ignored, one obtains the explicit expression:

$$L_f = \frac{6\kappa\lambda D_m}{d_f C(D_m)}, \tag{42}$$

where

$$\kappa = \frac{\ln[(1+a)/(1-a)]}{2a(f+k_3)}. \tag{43}$$

In the expression for a in Eq. (43), k_2 is set equal to zero.

In the case of the totally oriented nanowire, the mobility of the nanowire (Eq. (28)) for $\theta = 0$ is equated to the mobility of a sphere:

$$\frac{2ne\lambda}{\pi\eta d_f^2(\beta f + k_2)} = \frac{neC(D_m)}{3\pi\eta D_m}. \tag{44}$$

Solving for L_f, we find:

$$L_f = \frac{6\lambda D_m}{f d_f C(D_m)} - \frac{k_2 d_f}{f}. \tag{45}$$

For $L_f \gg \frac{k_2 d_f}{f}$, the following simplified expression is obtained:

$$L_f = \frac{6\lambda D_m}{f d_f C(D_m)}. \tag{46}$$

The two asymptotic expressions, Eqs. (42) and (46) differ by a constant with the predicted length in the aligned case larger by a factor of $(\kappa f)^{-1}$, which equals 1.88 for the accommodation factor $f = 0.9$. The dependence of L on D_m for the totally aligned case (Eq. (45)) is also plotted in Fig. 8.

4. Discussion

The experimental results are compared with the theoretical predictions in Table 1 and Fig. 8 at each applied voltage. It is seen that the experimental results fall between the two limiting cases of free rotation and totally aligned. For the shortest length, random orientation is favored, and the measured result agrees well with the limiting case of random rotation. As the length increases, the electrical energy is reduced for an oriented nanowire, which explains why measured results agree better with the prediction for a totally aligned nanowire.

Since we experimentally determined the diameter of the nanowires, another way of obtaining nanowire length is simply from the linear relation between D_m and D_A. Our prior experimental studies (Jung et al., 2004; Rogak et al., 1993) found that projected area diameter (D_A) is equivalent to the mobility diameter (D_m) from the free molecular regime to the transition regime ($D_m < 400$ nm) assuming free rotation of elongated fractal-like aggregates in an electric field. On the basis of the assumption of $D_A = D_m$, we calculated nanowire's length with the relation of $L_f = 0.25\pi D_A^2/d_f$. As seen in Fig. 8, the nanowire length determined by the relation of $D_A = D_m$ (marked as dashed line) was found to be between 17% and 23% greater than the predicted value for random orientation, Eq. (41). This comparison validates the functional form of L_f above for free rotation though with the constant 0.25 replaced by 0.21.

As one can see in Fig. 8 for nanowires longer than about 400 nm, the predicted length exceeds the measured value by almost a factor of two at 622 nm and then decreases to about 15% at 2674 nm. One possible reason is that the wires contained kinks and bends as observed in the TEM. Our theoretical analysis of the electrical energy is based on the total length of the nanowire, but a nanowire with bends would have a shorter moment arm, and therefore will feel a smaller torque than the equivalent straight wire. To verify the effect of this non-ideal structure of nanowires on mobility classification, we compute $P_1(x)$ given by Eq. (24) with β based on the nanowire effective length, defined as the longest chord measured from one end of the nanowire to the other. Automated TEM image analysis was used to analyze enough images (about 10 nanowires for each mobility) to provide a statistical meaningful average effective length. We found the following average effective lengths for each CNT group classified by the DMA: 95 ± 20 nm (470 V), 214 ± 40 nm (1089 V), 364 ± 70 nm (1607 V), 441 ± 150 nm (2199 V), 637 ± 200 nm (3169 V), and 787 ± 300 nm (4962 V), respectively. As one can see, the average effective length of CNTs classified by DMA turns out to be much shorter than total length of CNTs at the same applied voltage conditions (see Table 1). On the basis of this average effective length of CNTs, and accordingly modified $P_1(x)$, we predicted nanowire's length selected by DMA using the combination of Eqs. (34) and (37). The β multiplying f and k_3 in the denominator, which originates in the electrical

mobility (Eq. (28)), is approximated based on the total length rather than the effective length of the nanowire, because the drag on a cylinder is related to the total length (Eq. (27)). Using this approach, only one of the six data sets changed by more than a couple %, and in this case, $D_m = 100$ nm, the change was 8–9%.

We see that the modified moment arm analysis does not explain the difference between experiment and theory. Our analysis assumes that when the nanowire is aligned, $\theta = 0$ so that from Eq. (28) the mobility more than doubles from its minimum value. The actual nanowires have bends so the mobility will be decreased even when it is aligned, since much of the nanowire will be oriented at a nonzero angle. For example, for a long nanowire with an average orientation of 30°, the predicted length would decrease by 35–40%. A more detailed analysis of the dynamics of such structured nanowires would be required to validate our proposal that the discrepancy between measurement and theory is primarily from the enhanced drag force on the bent portions of the nanowire.

In Fig. 8, we have also plotted the nanowire length versus D_m considering only the effect of the charge in computing the orientation probability. It is seen that the polarizability term dominates for particle sizes larger than 80 nm. The apparent good agreement between the free charge computed curve and experiment is a fortuitous result of the theoretical analysis from assuming the nanowire to be straight. While the free charge energy is small compared to the polarizability term for these nanowires, it is likely the dominant term for a wide range of β for nanowires with diameters on the order of single walled CNTs.

Above we have provided a detailed model for the trajectory of nanowire through the DMA. It is also of interest to further develop the more empirical comparison made between the experimentally determined CNTs length and theoretically determined CNTs length in Fig. 7. The advantage of this approach is that it focuses on the orientation angle of the nanowire. One final step in this analysis is to compare the orientation-averaged mobility to the electrical mobility determined by the balance of electrical attraction and drag force (i.e. Eq. (28)). The orientation-averaged mobility in Eq. (34) for a given nanowire's aspect ratio and diameter is a function of radial location in the cylindrical DMA. The value of $\overline{Z_p(E,\beta)}$ changes with radial position in the DMA because of the change in the electric field. To account for this variation, we average $\overline{Z_p(E,\beta)}$ over the radial position as follows:

$$\overline{Z_p} = \frac{\int_{r_{in}}^{r_{out}} \overline{Z_p(E,\beta)}\,dr}{\int_{r_{in}}^{r_{out}} dr}. \tag{47}$$

In the same manner as done in Fig. 7, we first calculate the electrical mobility as a function of angle from the force balance (electrostatic and drag forces; i.e. Eq. (28)) for fixed values of β classified at each experimentally applied voltage in the DMA. Next we mapped the orientation-averaged mobility (i.e. Eq. (47)) at each experimental voltage, onto the graphs of the electrical mobilities (i.e. Eq. (28)). As seen in Fig. 9, the resulting effective angle of nanowires decreased with increasing β as expected. It is also noted that the resulting effective angle of rotating nanowires, determined by electrical mobility, was in good agreement with that determined by comparison between experimentally and theoretically determined nanowire's length as seen in Fig. 7. This indirectly justifies the validation of our theoretical approach in evaluating the orientation-average mobility.

We also apply our theoretical model to Moisala et al.'s (2005) experimental study, where length classification of SWNTs was conducted. They used a modified Hauke DMA geometry, and sheath/aerosol flow rate (i.e. $r_{in} = 2.5$ cm, $r_{out} = 3.3$ cm, $L_d = 11$ cm, $Q_{sh} = 14.9$ lpm, and $Q_a = 1.5$ lpm), and found that uniform diameter SWCNTs ($d_f = \sim 6.5$ nm) with total length of ~52 nm were classified at mobility size of ~23 nm in their DMA. Using their DMA operating conditions our model predicts a wire length of ~63 nm, which is close to their model prediction under the consideration of random orientation (~63 nm). This is also very close to the predicted nanowire length of 64 nm calculated by the linear relation of D_A and D_m (i.e. $L_f = 0.25\pi D_A^2/d_f = 0.25\pi \times (23\,\text{nm})^2/6.5\,\text{nm} = 64\,\text{nm}$). A possible reason of the deviation of nanotube's length determined by their experimental approach (~52 nm), and our theoretical model (~63 nm) is the uncertainty in their nanotube's diameter. They have taken the nanotube diameter as the average of SWCNTs' bundle diameters following mobility classification. In our model, it was found that the predicted nanowire length is very sensitive to nanowire's diameter. For instance, if $d_f \sim 7.5$ nm is taken as a SWCNT's diameter in our theoretical model, one obtains a nanowire length of ~53 nm, which is very close to SWCNT's length of ~52 nm observed by TEM analysis of Moisala et al. (2005). Either a precise control of nanowire diameter or precise knowledge is needed in order to accurately classify nanowire length.

Moisala et al. (2005) state that a perpendicular orientation of the nanotube relative to the direction of the electric field gives the best agreement with experiment. They go on to say that this orientation "is generally thought to be the

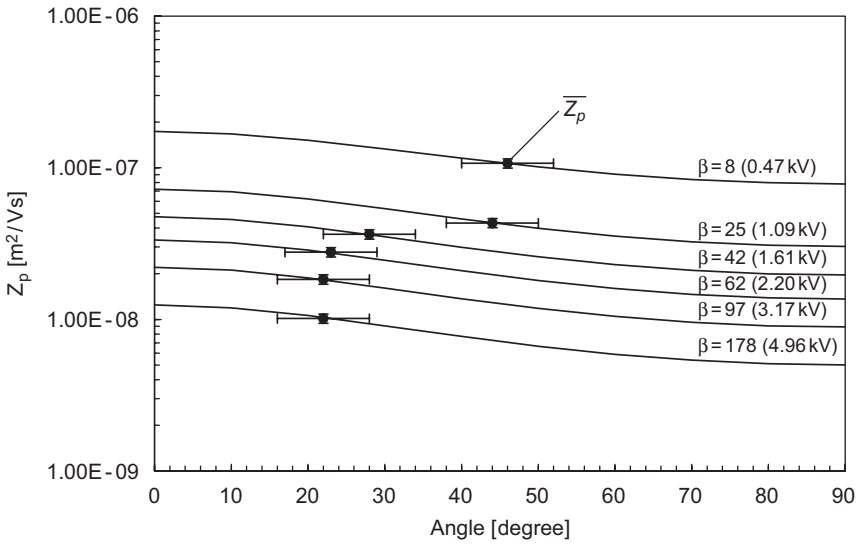

Fig. 9. Comparison between: (i) electrical mobility versus angle (i.e. Eq. (28)) for various values of β, each corresponding to a fixed voltage (given in parenthesis) and (ii) orientation-average electrical mobility (i.e. Eq. (47)) for experimentally determined CNTs aspect ratio.

most probable orientation for nonspherical particles in a DMA". Our theoretical study contradicts this conclusion. We predict that for SWCNTs such as this study (Moisala et al., 2005), the orientation would be random. As the diameter and aspect ratios are increased, the nanowires will preferentially align in the direction of the field both from the effect of the free charge and from the polarizability of the nanowire. In the free molecular limit, we do not find any condition that would favor a perpendicular orientation.

5. Summary and conclusion

To properly interpret the mobility size distribution of aerosol nanowires, the behavior of a charged nanowire in an electric field is needed. From a comparison between the electrical field energy and the thermal energy acting on a singly charged nanotube, it was found that the orientation of nanowires is strongly dependent on both the applied electric field strength, and the nanowires aspect ratio. Shorter nanowires ($\beta < \sim 30$) for a 15 nm diameter tend to rotate freely. However, the degree of alignment of longer nanowires ($\beta > \sim 30$) increased with increasing the electric field strength. The increased alignment results in a decreased drag force and an increased mobility. Thus, these longer nanowires are collected at a lower electric field than expected. The nanowire's length classified by a high voltage DMA electrode deviated significantly from that determined by the linear relation of D_A and D_m, which was found to be valid when mobility size, D_m, of randomly rotating fractal-like particle aggregates is less than 400 nm (Jung et al., 2004; Rogak et al., 1993).

In our theoretical model, the electrical mobility of rotating nanowire was derived from the balance of electrostatic attraction and drag forces acting on a rotating nanowire. The orientation averaged electrical mobility was derived based on a Boltzmann probability function. To predict the resulting nanowire's length selected by a cylindrical DMA, we have varied the nanowire's length until the nanowire's precipitating time was equal to the fluid transit time inside the DMA. Explicit expressions are obtained for the relationship between the nanotube length and the DMA size for the limits of random orientation and aligned orientation. By comparison of the theoretical model prediction with DMA-selected CNTs length, we found that the theoretical prediction over estimated the length for nanowires from 600 to 1000 nm by 40–50% and by 15–30% for the longer nanowires. We believe this discrepancy is a result of the bent structure of the experimental nanowires especially in regard to the increased drag on an "aligned" bent nanowire versus a straight nanowire.

In conclusion, a theoretical model has been derived for the behavior of a cylindrical charged particle undergoing Brownian rotation in an electric field. This theoretical model enables us to convert a mobility size distribution into a

length distribution of aerosol nanowires with uniform diameter in the free molecular regime. The methodology should be generic to other nanostructures with a high aspect ratio.

Appendix A

This Appendix A provides a derivation of the electrical mobility of a particle in the balance between fluid transit time and precipitation time.

Fluid transit time in the DMA is given as follows:

$$t_F = \frac{\pi(r_{out}^2 - r_{in}^2)L_d}{Q_{total}}. \tag{A.1}$$

And the precipitation time of a particle traveling from inlet slit to inner electrode (i.e. innermost trajectory) is given as follows:

$$t_{p,i} = \int_{r_{in}}^{r_a} \frac{dr}{v_r} = \frac{\ln(r_{out}/r_{in})}{2Z_p V_e}(r_a^2 - r_{in}^2). \tag{A.2}$$

From the combination of Eqs. (A.1) and (A.2), we obtain:

$$t_F = t_{p,i}, \tag{A.3}$$

$$Z_p = Q_{total}\frac{(r_a^2 - r_{in}^2)}{(r_{out}^2 - r_{in}^2)}\frac{\ln(r_{out}/r_{in})}{2\pi V_e L_d}, \tag{A.4}$$

where

$$Q_{sh} = Q_{total}\frac{(r_a^2 - r_{in}^2)}{(r_{out}^2 - r_{in}^2)}.$$

To find the location of inner and outer slit, one should first calculate the plug flow velocity as follows:

$$U_o = \frac{Q_{total}}{\pi(r_{out}^2 - r_{in}^2)}. \tag{A.5}$$

On the basis of the plug flow velocity (U_o), one can obtain the radii of r_a and r_b as follows:

$$Q_{sh} = U_o \cdot \pi(r_a^2 - r_{in}^2), \quad Q_a = U_o \cdot \pi(r_b^2 - r_{in}^2). \tag{A.6}$$

Under the DMA flow conditions of $Q_{sh} = 10$ lpm and $Q_a = 1$ lpm, we obtain $U_o = 19.67$ cm/s, $r_a = 1.891$ cm, and $r_b = 1.071$ cm.

Appendix B

This Appendix B provides a derivation of the approximate rotational mobility of cylindrical particles in free molecular regime.

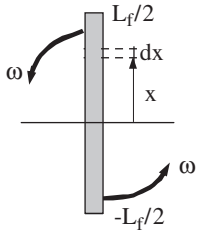

The average linear speed at a point x on a rod rotating at angular velocity ω is given by

$$v = \omega x, \tag{B.1}$$

where x is the distance from the center of fiber to the arbitrary position along axial direction.

The torque exerted on an increment of the cylinder length is estimated as

$$\mathrm{d}\tau = x\hat{i} \times \mathrm{d}\overline{F}_{\mathrm{rod}} = x\,\mathrm{d}F_{\mathrm{rod}} \sin\theta, \tag{B.2}$$

where

$$\mathrm{d}F_{\mathrm{rod}} = \frac{\mathrm{d}x}{L_{\mathrm{f}}} F_{\mathrm{rod}}.$$

The direction of the force is perpendicular to the length of the cylinder so that θ is equal to $\pi/2$. The expression for F_{rod} for the cylindrical portion omitting the end caps is given by

$$F_{\mathrm{rod}} = \frac{k\pi\eta d_{\mathrm{f}} L_{\mathrm{f}} v}{2\lambda}, \tag{B.3}$$

where

$$k = f + 2 - \left(\frac{6-\pi}{4}\right) f$$

Performing the integration, we obtain:

$$\tau = \int_0^{L_{\mathrm{f}}/2} \mathrm{d}\tau = \int_0^{L_{\mathrm{f}}/2} \frac{x F_{\mathrm{rod}}}{L_{\mathrm{f}}}\,\mathrm{d}x = \int_0^{L_{\mathrm{f}}/2} x \left(\frac{k\pi\eta d_{\mathrm{f}}\omega x}{2\lambda}\right) \mathrm{d}x$$

$$= \left(\frac{k\pi\eta d_{\mathrm{f}}\omega}{2\lambda}\right)\left(\frac{1}{3}x^3\right)_0^{L_{\mathrm{f}}/2} = \frac{k\pi\eta d_{\mathrm{f}}\omega L_{\mathrm{f}}^3}{48\cdot\lambda}, \tag{B.4}$$

The rotational mobility B_ω of a particle is defined as the ratio of the angular velocity to the torque resistance,

$$B_\omega = \frac{\omega}{\tau}. \tag{B.5}$$

From Eqs. (B.4) and (B.5), we obtain the final form of rotational mobility, B_ω, as follows:

$$B_\omega = \frac{48\lambda}{k\pi\eta d_{\mathrm{f}} L_{\mathrm{f}}^3} = \frac{48\lambda}{k\pi\eta d_{\mathrm{f}}^4 \beta^3}. \tag{B.6}$$

References

Baron, P. A., Deye, G. J., & Fernback, J. (1994). Length separation of fibers. *Aerosol Science and Technology*, *21*, 179–192.

Chen, B. T., Yeh, H. C., & Hobbs, C. H. (1993). Size classification of carbon fiber aerosols. *Aerosol Science and Technology*, *19*, 109–120.

Dahneke, B. E. (1973). Slip correction factors for nonspherical bodies-II free molecule flow. *Journal of Aerosol Science*, *4*, 147–161.

Deye, G. J., Gao, P., Baron, P. A., & Fernback, J. (1999). Performance evaluation of a fiber length classifier. *Aerosol Science and Technology*, *30*, 420–437.

Fuchs, N. A. (1964). *The mechanics of aerosols*. Oxford: Pergamon Press Ltd.

Griffiths, W. D. (1988). The shape selective sampling of fibrous aerosols. *Journal of Aerosol Science*, *19*, 703–713.

Hagwood, C., Sivathanu, Y., & Mulholland, G. (1999). The DMA transfer function with Brownian motion a trajectory/Monte-Carlo approach. *Aerosol Science and Technology*, *30*, 40–61.

Hoffman, J. D. (2001). *Numerical methods for engineers and scientists*. (2nd ed.), New York: Marcel Dekker.

Jung, H., Kittelson, D. B., & Zachariah, M. R. (2004). Kinetics and visualization of soot oxidation using transmission electron microscopy. *Combustion and Flame*, *136*, 445–456.

Kim, S. H., & Zachariah, M. R. (2005). In-flight size classification of carbon nanotubes by gas phase electrophoresis. *Nanotechnology*, *16*, 2149–2152.

Kim, S. H., & Zachariah, M. R. (2006). In-flight kinetic measurements of the aerosol growth of carbon nanotubes by electrical mobility classification. *Journal of Physical Chemistry B*, *110*, 4555–4562.

Kim, S. H., & Zachariah, M. R. (2007). Gas-phase growth of diameter-controlled carbon nanotubes. *Materials Letters*, *61*, 2079–2083.

Knutson, E. O., & Whitby, K. T. (1975). Aerosol classification by electric mobility: Apparatus, theory, and applications. *Journal of Aerosol Science*, *6*, 443–451.

Lipowicz, P. J., & Yeh, H. C. (1989). Fiber dielectrophoresis. *Aerosol Science and Technology*, *11*, 206–212.

Moisala, A., Nasibulin, A. G., Shandakov, S. D., Jiang, H., & Kauppinen, E. I. (2005). On-line detection of single-walled carbon nanotube formation during aerosol synthesis methods. *Carbon*, *43*, 2066–2074.

Rogak, S. N., Flagan, R. C., & Nguyen, H. V. (1993). The mobility and structure of aerosol agglomerates. *Aerosol Science and Technology*, *18*, 25–47.

Song, D. K., Lenggoro, I. W., Hayashi, Y., Okuyama, K., & Kim, S. S. (2005). Changes in the shape and mobility of colloidal gold nanorods with electrospray and differential mobility analyzer methods. *Langmuir*, *21*(23), 10375–10382.

Stöber, W. (1972). Dynamic shape factors of nonspherical aerosol particles. In: T. T. Mercer, P. E. Morrow, & W. Stöber (Eds.), *Assessment of airborne particles* (pp. 249–289). Springfield, IL: Charles C. Thomas.

Timbrell, V. (1972). An aerosol spectrometer and its applications. In: T. T. Mercer, P. E. Morrow, & W. Stöber (Eds.), *Assessment of airborne particles* (pp. 290–330). Springfield, IL: Charles C. Thomas.

Zebel, G., Hochrainer, D., & Boose, C. (1977). A sampling method with separated deposition of airborne fibres and other particles. *Journal of Aerosol Science*, *8*, 205–213.

Further reading

Wolfram Research Inc. (2003). *Mathematica* (Computer Software).